CoCO2
Prototype system for a Copernicus CO_2 service

Quantification of transport errors and database of optimized fluxes and simulations for an ensemble of models and inversion set-up

Antoine Berchet

coco2-project.eu

Co-ordinated by ECMWF

CoCO2

Prototype system for a Copernicus CO_2 service

D5.3 Quantification of transport errors with an ensemble of inversions

Dissemination Level:	Public
Author(s):	Antoine Berchet (CEA / LSCE) Joël Thanwerdas (Empa) Eldho Elias (MPI-BGC) Friedemann Reum (DLR) Grégoire Broquet (CEA / LSCE)
Date:	30/09/2023
Version:	0.1
Contractual Delivery Date:	30/09/2023
Work Package/ Task:	WP5/ T5.3
Document Owner:	CEA
Contributors:	CEA, Empa, DLR, MPI-BGC
Status:	Final

CoCO2: Prototype system for a Copernicus CO_2 service

Coordination and Support Action (CSA)
H2020-IBA-SPACE-CHE2-2019 Copernicus evolution – Research activities in support of a European operational monitoring support capacity for fossil CO2 emissions

Project Coordinator: Dr Richard Engelen (ECMWF)
Project Start Date: 01/01/2021
Project Duration: 36 months

Published by the CoCO2 Consortium

Contact:
ECMWF, Shinfield Park, Reading, RG2 9AX,
richard.engelen@ecmwf.int

The CoCO2 project has received funding from the European Union's Horizon 2020 research and innovation programme under grant agreement No 958927.

Table of Contents

Figures

Tables

1 Executive Summary

This documents presents results from the inter-comparison of inversions of CO2 NEE surface fluxes over Europe assimilating the CO2 observations from the continuous surface network, using different atmospheric transport models and inversion approaches, but systematically carried out using the Community Inversion Framework (CIF). CIF allows to compute inversions using different atmospheric transport models and inversion approaches, with the guarantee of consistency within all application cases, in terms of algorithms for the common components of the inversion problem. The consistency includes fully consistent definition of the control vector (resolution, scale, structure of uncertainties), and the observation vector (including data selection and observational errors specified in the inversion), common pre-processing, operations within the inversion computations, as well as post-processing. We carried out inversions with the models LMDZ, CHIMERE, STILT, ICON-ART and WRF-Chem, with the variational and the Ensemble Square Root Filter methods, all the parameters not directly linked to these models and approaches being identical. The raw differences between inversions from one model to the other, or from one method to the other, at the model and inversion resolutions are large. The aggregation of the results at larger scales (e.g., over countries, or group of countries) are much more consistent across the different inversions. Our results are a break through compared to previous inter-comparison exercises as differences can precisely be attributed to transport and/or methodological uncertainties . We conclude that for the European CO2 inversions, the denser part of the surface observation network (in France, Germany, Scandinavia, and British Isles) is sufficient to limit the impact of transport and methodological uncertainties on inversion results. Conversely, in regions with sparse networks, such as in the Iberian and Italian peninsulas, inversion results are very uncertain, due to large spread between inversion methods and transport model. The Community Inversion Framework will be used in the future to conduct traceable and systematic inversions applied to different scales and regions of the world, different species, including CH4 and N2O in particular, and different data streams (including satellite platforms).

2 Introduction

2.1 Background

Transport errors represent one of the largest sources of uncertainties in atmospheric inversions. They impair our ability to compare observations with simulations in a consistent and suitable way. Yet, their quantification, and even more, the quantification of the error in the flux estimates due to these errors, proved very challenging in the past because research groups performing inverse modelling experiments can usually only afford to employ one specific transport model in their inversion system because these groups have developed inversion system around a specific and thus single transport model. Using different transport models driven by different inversion systems, with inversion set-ups and intermediate operations not fully consistent with each other, it was difficult to unequivocally attribute errors in the flux estimates to transport only, and not to the inversion system as a whole. Still, such estimates have been the cornerstone of the practices within inversion community for more than two decades, with long-term inter-comparison efforts, such as the TRANSCOM exercise, which over the course of the years allowed to improve community practices and identify fix deficiencies and caveats in inversion (Engelen et al., 2002; Gurney et al., 2002; Law et al., 2003; Gurney et al., 2003; Baker et al., 2006; Patra et al., 2011; Peylin et al.,2013; Basu et al., 2018; Chevallier et al., 2019). Similarly, inversion groups often use different data assimilation methods to solve their inversion cases. Most inversion teams rely on either variational inversion or ensemble-based inversions, with their strengths and caveats, but potentially inducing methodological uncertainties due to different approximations in all methodological approaches

We propose to take full advantage of a new community tool, the Community Inversion Framework (CIF) to rigorously assess the impact of transport and methodological errors in the present task. CIF was developed during the H2020 project VERIFY as an open-source flexible research suite for inversion studies. The main purpose behind this new numerical system was to rationalize development efforts within the inversion community by bringing existing systems together within a unified standardized system, sufficiently flexible to manage the connection between traditional inversion approaches (analytical, ensemble based and variationnal), to the whole range of atmospheric transport models used in the community (CHIMERE, LMDZ, FLEXPART, STILT, TM5, ICON-ART, WRF-Chem). CIF was applied on test cases at the regional scale in Europe in the project VERIFY with a variety of models (CHIMERE and FLEXPART for CH4). Here, the objective is to clearly identify the impact of transport uncertainties, as well as methodological uncertainties on retrieved fluxes. To do so, we designed a strict protocol with identical input, configuration and processing of outputs. We chose the year 2019 for CO2 NEE fluxes in Europe, using surface observations to carry out uncertainty quantification using different models (in particular, a set of Eulerian models and one Lagrangian model, and regional and global models, as well as online and off-line models in terms of computation of meteorological forcing fields) in different inversion set-ups, including the underlying data assimilation method (variational and ensemble methods).

2.2 Scope of this deliverable

2.2.1 Objectives of this deliverables

The objective of this deliverable is to describe the inter-comparison exercise carried out in CoCO2 using the Community Inversion Framework for CO2 NEE fluxes at the regional scale in Europe using surface observations. We describe the system used for the inter-comparison, the overall protocol and data exchange process, as well as results from the inter-comparison exercise.

2.2.2 Work performed in this deliverable

Dedicated technical developments in CIF were carried out for the present deliverable. Numerous inversions and simulations were performed to reach the objective of the deliverable.

In particular, at the beginning of the CoCO2 project, ICON-ART and WRF-Chem were not implemented in CIF. STILT was not included neither, but as a Lagrangian model, we used the same outline as the implementation of FLEXPART, but generalizing the reading of footprints to STILT footprint format.

2.2.3 Deviations and counter measures

Staffing issues limited the scope of the inter-comparison, in particular in terms of the number of transport models used in the inter-comparison. We originally planned to include the FLEXPART, LOTOS-EUROS and TM5 atmospheric transport models. TM5 and FLEXPART have been fully implemented in CIF but could not be run within the framework of CoCO2. LOTOS-EUROS could not be implemented in CIF during the project. Nevertheless, as a trade-off effort, STILT (which was not originally planned in T5.3) was implemented and used thanks to dedicated efforts by MPI-BGC.

Thanks to optimization in the system, we could extend the durantion of the experiments. Originally, only short periods were targeted, but optimization in the system allowed us to compute full year inversions, hence covering a full seasonal cycle.

3 The Community Inversion Framework

3.1 Background

The Community Inversion Framework (CIF; community-inversion.eu) was initially designed in the frame of the H2020 project VERIFY (verify.lsce.ipsl.fr) in 2018 (Berchet et al., 2021). The rational for such a community to be developed was to bring the European inversion community together and benefit from the variety of inversion systems in Europe, while avoiding duplicated developments and technical efforts. The system was built as a flexible Python library (Berchet et al., 2022) able to apply atmospheric inversions using a large number of models, with different inversion methods, and with as many data streams as possible.

CIF was used at the end of VERIFY for an inter-comparison of CH4 inversions over Europe based on surface observations of methane (CH4), with the model CHIMERE and two version of the model FLEXPART, and using a variational inversion approach (see VERIFY deliverable D4.10).

3.2 Inversion methods in CIF

The purpose of Bayesian inversions is to retrieve posterior fluxes, considering observations and using information on atmospheric transport and chemistry from a chemistry-transport model. The approach can be summarized by the following system of equations:

$$\begin{cases} p(x \mid y) \sim p(y \mid x) \cdot p(x) \\ p(x) \sim N(x_b, B) \\ p(y \mid x) \sim N(y^o, R) \end{cases}$$

Equation 1. Bayes theorem applied to atmospheric inversions with Gaussian assumptions.

Where x are the flux variables to be optimized, x_b represents prior fluxes to be used in the inversion, y^o the observations to be used and R and B the covariance matrices of uncertainties in the observation and control space respectively.

Under Gaussian assumption for the prior control and observation errors, the posterior distribution of fluxes $p(x|y)$ is a normal distribution $N(x_a, P_a)$, with x_a the posterior fluxes and P_a the posterior uncertainties on fluxes.

x_a and P_a are described explicitly by the following set of equations

$$\begin{cases} x_a = x_b + K(y^o - Hx_b) \\ P_a = B - KHB \end{cases}$$

Equation 2. Solution to the Bayes equations.

with H the observation operator linking fluxes to observations, including the transport model, but also intermediate operations, such as flux regridding, temporal interpolations, etc.

These equations usually cannot be solved analytically as matrices (especially H) cannot be built explicitly and matrix inversions cannot be computed in very high dimensional problems with millions of unknown fluxes and tens of thousands of observations.

To obtain posterior fluxes, numerical data assimilation methods are used. In CIF, the variational approach and the Ensemble Square Root Filter are implemented. Other technics exist, implying e.g. smart approximations of the problem such as in Yadav and Michalak (2013). As of today, only the variational and EnSRF approaches are implemented in CIF, as the two main approaches used in the community. Nevertheless, the flexibility of CIF and its cooperative nature leaves open the door for future implementation of other inversion technics.

3.2.1 Variational approach

One possible way to avoid the dimension issue is the variational approach. We shorten it as 4D-VAR in figures. Computing the normal distribution in Eq. (2) is equivalent to finding the minimum of the cost function:

$$J(x) = \frac{1}{2}(x - x_b)B^{-1}(x - x_b) + \frac{1}{2}$$

This cost function can be minimized using quasi-Newtonian descending algorithms based on the gradient of the cost function:

$$\nabla J_x = B^{-1}(x - x_b) + H^T\left(R^{-1}(y^o - Hx_b)\right)$$

For the present task, we used the algorithm M1QN3 (Gilbert and Lemaréchal, 1989), specifically designed to solve large minimization problems.

Variational inversions rely on the adjoint code of the transport model, which is not always available. CHIMERE and LMDZ have been co-developed with their adjoint code. WRF-Chem and ICON-ART can only compute forward computations. STILT, as a Lagrangian model, is a so-called auto-adjoint model, making it straightforward to compute variational inversions.

3.2.1.1 Ensemble Square-Root Filter (EnSRF)

The implementation of the Ensemble Square-Root Filter in CIF is based on the CTDAS system (van der Laan-Luijkx, 2017). In such system, the issue with high dimension in the system of Eq. (2) is avoided using three main procedures:

- observations are assimilated sequentially in the system to reduce the dimension of the observation space, making it possible to compute matrix products and inverses.
- covariance matrices are approximated with a Monte Carlo ensemble of possible control vectors.
- the overall inversion window is chunked into moving windows for which an ensemble forward simulation is done to solve for fluxes for that period, then updates on concentrations are propagated to the next moving window after optimization of fluxes.

In our case, the moving windows last 20 days with a step of 10 days between each window, hence allowing each 10-day interval to be optimized by 20 days of observations.

EnSRF is used with the models ICON-ART, WRF-Chem and CHIMERE, with CHIMERE being used as well with the variational, thus allowing to evaluate the impact of the method on results.

3.3 Available models in CIF, used in the present study

3.3.1 CHIMERE

CHIMERE (see https://www.lmd.polytechnique.fr/chimere/) is a non-hydrostatic Eulerian chemistry-transport model. Its area-limited domains can be designed to cover the hemispheric to the urban scales, with horizontal resolutions from several degrees to one kilometer. The time-steps usually cover a few minutes, depending on the CFL and choices made by the user for minimizing computation costs. For the purpose of flux inversions, the tangent-linear and the adjoint codes have been developed and parallelized, only for trace-gases (see Fortems-Cheiney et al., 2021, their Section 3.2 for more details). The required input data are meteorological 3D and 2D fields (e.g. temperature, wind speed), boundary conditions for concentrations at the four sides and at the top of the domain and emission fluxes. The comparison to surface measurements is done by extracting from the model the simulated concentrations in the grid cell matching the stations' locations for the time-steps matching the measurement date and time. If the measurement covers a longer time (e.g. hourly means from continuous measurements), the simulated concentrations for the matching time-steps are

averaged. For this deliverable, CHIMERE was run using meteorological data from the ECMWF's IFS operational forecast (every three hours) retrieved at 0.25° × 0.25° and interpolated onto the model's grid (0.5° × 0.5°). CHIMERE extends from the surface to 200 hPa with 17 sigma-pressure levels.

CHIMERE has been implemented in CIF and is currently used at the regional scale over Europe and East Asia with greenhouse gases (CO2, CH4, N2O) and chemically active species (NOx, CO). It is also used at finer scale at the national scale over France, in particular in T4.4 and T5.4 of WP4 and WP5 of CoCO2 respectively.

3.3.2 STILT

STILT (Stochastic Time-Inverted Lagrangian Transport) is a Lagrangian transport model that can simulate atmospheric transport and derive the sensitivity of the measurement locations to the underlying fluxes (Lin et al., 2003). An ensemble of virtual particles, representing an air parcel, is transported under the influence of advection and turbulent mixing in the atmosphere. In STILT, the air parcel is represented as particles of equal mass which are transported along a trajectory with the mean and random velocities generated using a Markov chain process. Lagrangian transport models have the ability to resolve atmospheric transport on sub-grid scales, which is expected to reduce the transport uncertainties associated with the finite grid restrictions. For this study, meteorological fields from the European Centre for Medium-Range Weather Forecasts (ECMWF) for 2019 are used to simulate tracer transport over the European domain. Specifically, we use short term forecasts extracted at a 0.25° x 0.25° horizontal and 3-hourly temporal resolution. The sensitivity "footprints" generated by STILT are then used in CIF for the forward simulations and the inversions.

3.3.3 ICON-ART

The Icosahedral Nonhydrostatic (ICON) Weather and Climate Model (Zängl et al., 2015) is a joint project between the Deutscher Wetterdienst (DWD), the Max-Planck-Institute for Meteorology (MPI-M), the Deutsches Klimarechenzentrum (DKRZ) and the Karlsruhe Institute of Technology (KIT) for developing a unified next-generation global numerical weather prediction (NWP) and climate modeling system. The ICON modeling framework became operational in DWD's forecast system in January 2015. In addition, ICON is being deployed for numerical forecasting for the Swiss meteorological service, MeteoSwiss. It will replace the COSMO forecasting model that is currently being used.

The Aerosols and Reactive Trace gases module (ART), developed and maintained by KIT, supplements ICON to form the ICON-ART model, by including emissions, transport, gas phase chemistry, and aerosol dynamics in the troposphere and stratosphere.

ICON-ART is a non-hydrostatic Eulerian chemistry-transport model. Its horizontal domain is described by an icosahedral grid and can cover either the globe or a limited area, ranging from several degrees to a few kilometers. For this intercomparison, a horizontal resolution of 26 km (~0.35 degrees) is adopted. The vertical domain extends from the surface to an altitude of 23 km, with 60 levels described by a height-based terrain-following vertical coordinate. Meteorological fields (e.g. temperature, wind speed) are computed online by the ICON model and, at Empa, several prognostic variables (e.g. temperature, wind speed, specific humidity…) are nudged towards the ERA5 reanalysis data provided by the ECMWF at a 3-hourly time resolution. This prevents the model from drifting away from a realistic atmospheric state. The ERA5 data is also used to initialize the model. For the limited-area mode, boundary conditions can be prescribed at the borders of the domain using external data. Emission fields for any transported species are processed by the Online Emissions Module (OEM; Jähn et al., 2020), included in ART. Output instantaneous concentrations are written at hourly resolution and are

temporally, vertically and horizontally interpolated offline in order to retrieve simulated equivalents of observations.

3.3.4 WRF-Chem

The Weather Research and Forecast (WRF) is a numerical weather prediction model developed at NCAR (National Center for Atmospheric Research) in Boulder, Colorado (Skamarock et al. 2021). WRF-Chem is the online chemistry module coupled to WRF (Grell et al. 2005). WRF supports a wide range of scales, from global simulations down to Large Eddy Simulations. Here, we use WRF version 4.4 and the passive tracer module of WRF-Chem, also called WRF-GHG (Beck et al. 2011). For the intercomparison, WRF is driven by ERA5 fields (Hersbach et al. 2023) updated every three hours. ERA5 is used for the initial conditions, boundary conditions and continuously nudging the WRF weather solution inside the domain. The simulation is run at 0.5 degree horizontal resolution with 49 vertical levels up to 50 hPa, and a timestep of two minutes. Outputs are written hourly, which are then sampled and interpolated by CIF.

3.3.5 LMDZ

LMDZ is the atmospheric component of the Institute Pierre-Simon Laplace Coupled Model (IPSL-CM) which significantly contributed to the last three IPCC assessment reports. The configuration is the one developed and used for the sixth phase of the Coupled Model Inter-comparison Project (CMIP6), except that horizontal winds are nudged to the winds analysed by ECMWF, and that the transport mass fluxes are computed once and for all, before being used off-line for tracer transport. This version has a regular horizontal resolution of 2.50^o in longitude and 1.27^o in latitude, with 79 hybrid layers in the vertical. Current or previous versions of LMDZ have participated in the most recent tracer transport model intercomparisons (e.g., Crowel et al., 2019). A detailed evaluation of the current version can be found in Remaud et al., 2018.

3.4 Developments in CoCO2

Despite the overall maturity of the CIF at the end of the project VERIFY, further developments were needed in the framework of CoCO2 to carry out a full inter-comparison. Developments included:

- Integration of additional models in CIF:
  - STILT was integrated as an extension of the FLEXPART plugin, as Lagrangian models are very similar in structure; only the reading of STILT footprints was changed compared to FLEXPART original plugin
  - ICON-Art and WRF-Chem were integrated in CIF as Eulerian models. Considering the large data files produced by these models, dedicated optimization had to be done to accommodate them into CIF
- Integration of the Ensemble Square Root Filter method: this was done with contributions from Empa, FMI and DLR. The integration is based on the existing system CTDAS (van der Laan-Luijkx et al., 2017) with dedicated optimizations and generalizations; we replicated their approach and adapted their codes to fit CIF standards and interfacing.
- Generalization of input processing: CIF can now accommodate most emission and 4D-fields provided as standard NetCDF files, including reading and regridding them to required resolution as transport model inputs; such feature guarantee the full consistency of surface fluxes and boundary conditions in our experiments with different transport models.. No pre-formatting is now required to use such files in CIF and

regridding and temporal resampling is automatically carried out online with CIF simulations.

4 Inter-comparison inversion protocol

4.1 Inversion of CO2 fluxes in Europe

For our inter-comparison, we rely on the history of European inter-comparisons dedicated to CO2 fluxes (e.g., Monteil et al., 2020). Our work is a continuation and refinement of past studies. Our purpose is to assess natural terrestrial CO2 fluxes over a domain covering all continental Europe, the British Isles and Scandinavia. For that purpose, we use surface observations, as provided by the ICOS network. In particular, Net Ecosystem Exchanges (NEE) are very uncertain in their magnitude and seasonal timing.

We propose to assess the impact of transport and methodological uncertainties on retrieve seasonal timing and magnitude of NEE fluxes.

4.2 Protocol overview

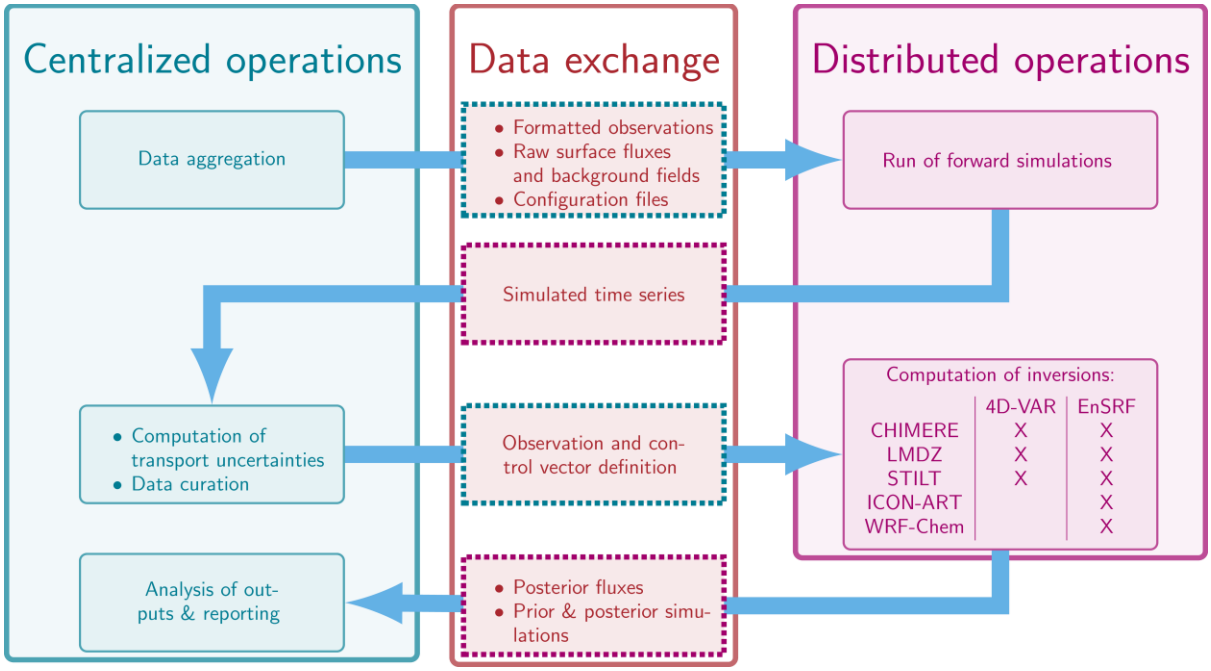

Figure 1: Inversion protocol. Centralized operations are carried out at LSCE. Distributed operations are carried out by partners at MPI-BGC, Empa, DLR, and LSCE.

Figure 1 shows the overall protocol and exchanges between the coordination (LSCE) and other partners (Empa, DLR, MPI-BGC).

First, data are collected by the coordination. Regarding observations, available observations are aggregated and formatted to a single file compatible with CIF. Other inputs (surface fluxes, 4D fields used for boundary and initial conditions) are not pre-formatted. Contrary to other inter-comparison exercises, using the capability and flexibility of CIF, it is possible to distribute raw input data as such and guarantee a consistent processing of such inputs to regridded and reformatted model inputs.

Partners then run forward simulations to compute simulated equivalents to observations.

Simulated equivalents from various models are compared and aggregated to compute consistent transport errors to be used in inversions.

Curated observations, as well as observational errors and inversion configuration, are sent back to partners for distributed computation of inversions.

Inversion results are stored in a consistent format by CIF, making the post processing and analysis of results painless and transparent. No extra processing and regridding is to be done by neither the partners nor the coordination for the processing of results, contrary to classical inter-comparison with numerous inversion systems.

4.3 Transport error and inversion method uncertainties

The main purpose of Task 5.3 was to assess inversion uncertainties arising from transport errors as well as from the method used to retrieve fluxes. Transport errors are quantified by running inversions using several transport models inside CIF, whereas method uncertainties are quantified by using different inversion solvers for which we only used CHIMERE. We detail below the models used in our study as well as inversion methods. The combinations of transport models and inversion methods used in our inter-comparison are detailed in Table 1.

Table 1. Summary of inversions carried out in the task.

		Inversion method	
		variational	**EnSRF**
Transport model	CHIMERE	X	X
	LMDZ	X	
	STILT	X	
	ICON-ART		X
	WRF-Chem		X

5 Standardized inversion set-up

In the present section, we present the common standardized set-up used in the inversion experiments.

5.1 Input data

Our inversion set-up is based on classical CO2 inversion configurations as used in previous inter-comparison exercises, such as EUROCOM (Monteil et al., 2020), or VERIFY (McGrath et al., 2023). We detail below each category of input: observations, surface fluxes, meteorology, and global concentration fields used as background and initial conditions for our transport simulations

5.1.1 Observations

Our inversions use observations of CO2 atmospheric mixing ratios in Europe. We use the most recent data “European Obspack 2023-1 for CO2 and CH4” (ICOS RI, 2023) in our inversions. It includes continuous measurements from 58 stations over Europe. For the year 2019, 47 stations are available (see Figure 2).

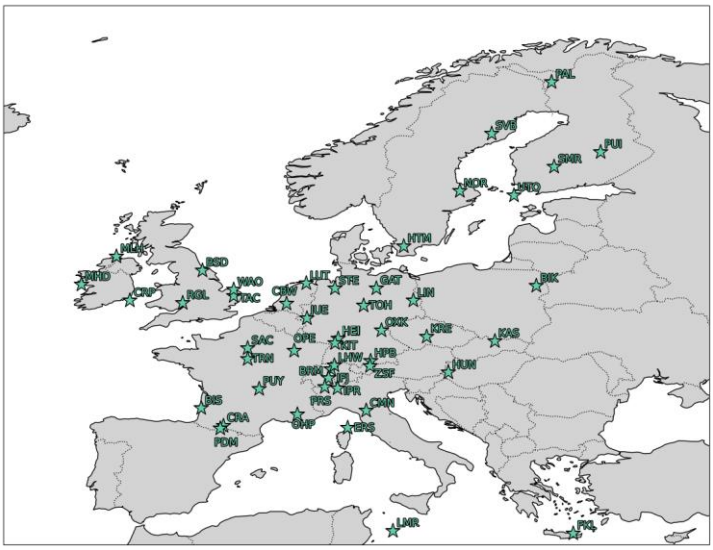

Figure 2. Map of available observation sites in 2019.

5.1.2 Surface fluxes

Surface fluxes are computed as the sum of anthropogenic fluxes, terrestrial ecosystem fluxes (more specifically: the Net Ecosystem Exchange - NEE), and oceanic fluxes. Biomass burning emissions are neglected in our study. We optimize NEE only in our case (see Sect. 5.2.1)

5.1.2.1 Anthropogenic fluxes

The anthropogenic CO2 emissions, considered as perfect and consequently not optimized in the inversions, are based on the spatial distribution of the EDGAR-v4.2 inventory, on national and annual budgets from the BP (British Petroleum) statistics and on temporal profiles at hourly resolution derived with the COFFEE approach (Steinbach et al., 2011, available on the ICOS Carbon Portal). The data is provided at 0.1°x0.1° horizontal resolution and hourly temporal resolution.

5.1.2.2 Biogenic fluxes

Biogenic fluxes are deduced from ORCHIDEE simulations. We use two sets of simulations: global simulations from the TRENDY project and higher resolution simulations from the project VERIFY over Europe.

1. ORCHIDEE-TRENDY simulation is performed in the context of the TRENDY model-intercomparison project. This simulation is forced with the set of inputs distributed within the project: CRUERA atmospherical climate forcing (global, 6-hourly, 0.5-degree), LUH2 land-use change dataset, CO2 global atmospheric concentration data, Nitrogen fertilizer input datasets. All TRENDY simulations follow a unified protocol: model spinup re-cycling forcing from 1901-1920 with other input data from 1700 until reaching the equilibrium of model carbon pools (340 years of spinup in case of ORCHIDEE), transient simulation for 1700-1900 varying CO2 and land-use data but still recycling climate forcing, historical simulation for 1901-2020 varying all data inputs.
2. The ORCHIDEE-VERIFY simulation is performed in the context of the VERIFY project over European region. This simulation is forced with the CRUERA dataset, which is the meteorological forcing derived from the ERA5-Land dataset (originally global, 1-hourly, at 0.1-degree resolution), transformed to the VERIFY region of interest (35N:73N, 25W:45E, 3-hourly, at 0.125-degree resolution) and re-aligned with the CRU observation dataset (for air temperature, shortwave radiation, humidity and precipitation). For the land use the Hilda+ dataset is used, for the nitrogen inputs - the

EMEP model outputs. The VERIFY simulation is done following the general protocol used in the TRENDY project.

5.1.2.3 Ocean fluxes

The ocean prior fluxes come from a hybrid product of the University of Bergen coastal ocean flux estimate and the Rödenbeck global ocean estimate (Rödenbeck et al., 2014). The data is provided at 0.125°x0.125° horizontal resolution and at daily temporal resolution.

5.1.3 Meteorological fields

Transport models need meteorological forcings for their computations. The models used for our inter-comparison are based on a not fully consistent approach to generate meteorological inputs. In all cases, the original meteorological forcing come from ECMWF products (ERA5 in most cases, operational forecasts in the case of CHIMERE), but with different processing. The different approaches is one cause of transport errors as the driving fields are not fully identical between transport models.

ICON-ART and WRF-Chem are so-called online systems that compute meteorological fields on-the-fly. As they are regional models, they need boundary conditions for meteorology, that are deduced from the ERA5 dataset in both cases.

Other models are off-line models which use pre-computed meteorological forcing interpolated from external datasets. STILT uses meteorological fields from ERA5 interpolated at 0.1° resolution. LMDZ uses pre-computed mass fluxes from the online GCM full version of LMDZ, nudged to ERA5 data. CHIMERE uses ECMWF forecasts interpolated at 0.5° resolution.

5.1.4 Background concentration fields

Initial, lateral and top boundary conditions for CO2 mole fractions are generated from the new CAMS global CO2 inversions v20r2 (Chevallier et al., 2010). The data is provided at a resolution of 2.50º in longitude and 1.27º in latitude and 3-hourly temporal resolution. For LMDZ global simulations, we use CAMS posterior fluxes outside of the European domain for the sake of consistency with the background used in the other models.

5.2 Inversion configuration

5.2.1 Definition of the control vector

The control vector contains variables to be optimized by the inversion. In our case, we optimize NEE only at the pixel scale at the original resolution of ORCHIDEE-VERIFY of 0.1°x0.1°. This resolution is higher than those of the transport models. We chose such a definition to ensure that the original data set is optimized, independently of their resolution. CIF automatically computes the needed regridding from the ORCHIDEE resolution to the model resolutions. We decided not to optimize for boundary conditions, even though it is an acknowledge issue in regional inversions. We do so first as we use state-of-the-art global CO2 fields from CAMS55, optimized using surface measurements, thus limiting possible discrepancies with real background concentrations, second as the purpose of the present task is to analyse the impact of transport errors. The impact of background errors needs to be discussed in dedicated spin-off works to cover all aspects of uncertainties in inversions.

We optimize scaling factors with a temporal resolution of 10 days, with no temporal correlations of errors. Still, as classically done in CTDAS applications (e.g., van der Laan-Luijkx et al., 2017), propagation weights are applied from one assimilation step to the next one in the EnSRF cases.

5.2.2 Definition of the observation vector

The observation vector is directly defined from hourly measurements as provided in the ICOS ObsPack dataset (ICOS RI, 2023), containing high accuracy CO2 dry air mole fractions from 58 ICOS and non-ICOS European observatories. We do not select all available data, but instead keep only afternoon values for near-surface and coastal sites, and night-time values for mountain sites.

While afternoon hours are defined as times from 12:00 to 16:00 UTC, night-time hours for mountain sites are times from 00:00 to 04:00 UTC.

5.2.3 Definition of uncertainties

5.2.3.1 Model-data mismatch

We describe the uncertainty in observation space (R) as a combination of instrument uncertainty and transport model uncertainty. Using the spread of the models in their contribution from the background and the surface fluxes, it is possible to compute the observation uncertainty that is used for the inversion. For a given observation point, we use the formula:

$$\epsilon_{tot}^2 = \epsilon_{obs}^2 + \epsilon_{emis}^2 + \epsilon_{bg}^2$$

with ϵ_{emis} the standard deviation of simulations from surface fluxes, ϵ_{bg} the standard deviation of simulations from the background and ϵ_{obs} the instrument error as specified in the raw observation files. Covariances between observational errors were ignored.

5.2.3.2 Control vector uncertainties

Uncertainties in the control vector are deduced from the values of respiration as given in the ORCHIDEE-VERIFY dataset over Europe at 0.1x0.1° resolution, similarly to what is classically done in CO2 inversions over Europe (e.g., Broquet et al., 2013; Monteil et al., 2020). The uncertainties standard deviation is computed as 100% of the respiration flux for each land pixel. We also apply non-diagonal terms on the control vector uncertainty covariance matrix using isotropic spatial correlations with an e-fold decreasing correlation using a correlation length of 200 km (see Broquet et al., 2013). The number of spatial degrees of freedom per 10-day window thus amounts to 15188.

6 Results

6.1 Forward simulations and comparison of models

The initial step in the inter-comparison involved distributing reference data files and adapting configuration files to run forward simulations with all models. Figure 3 shows examples of simulated time series at the observation sites NOR and SMR. At first glance, all models are in agreement with the observations and with each other, although deviations can reach a few ppm.

Running separate simulations with no background or no surface fluxes in the domain of transport simulations allows us to separate the influence of the background at the observation sites, as well as the contribution from surface fluxes inside Europe. Figure 4 illustrates examples of the background simulations, while Figure 5 displays time series of flux contributions. In general, all five models are in agreement regarding the background and surface flux contributions.

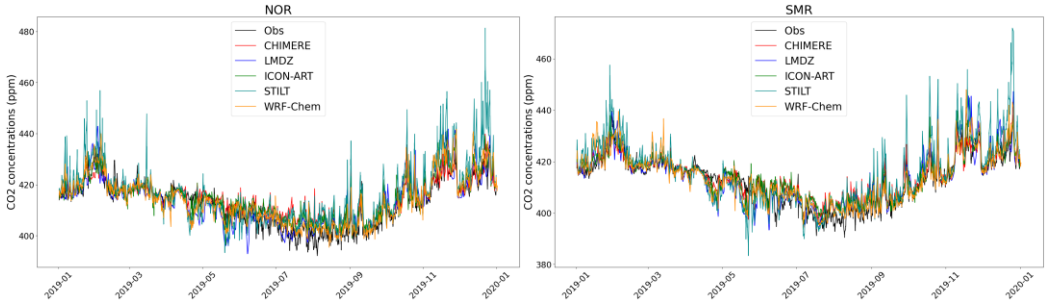

Figure 3. Example of hourly simulated (using prior fluxes) and observed time series at two observation sites (NOR and SMR) for afternoon times.

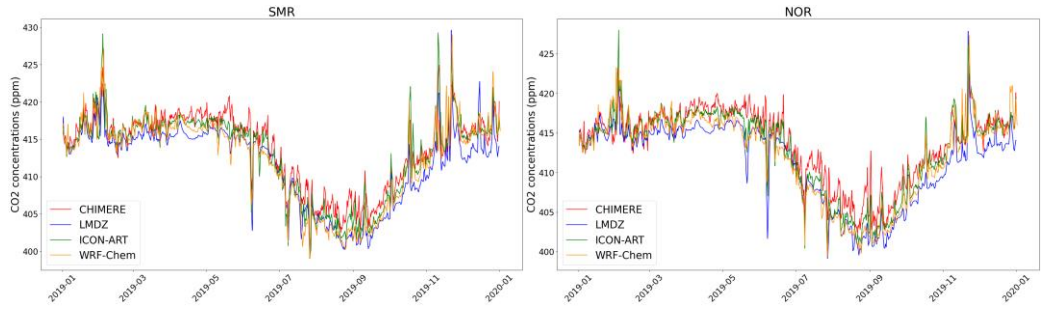

Figure 4. Example of simulated influence of the background at NOR and SMR. Same as Figure 3.

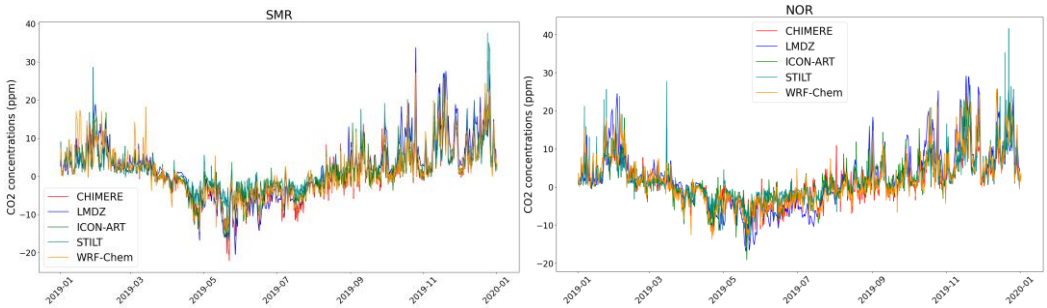

Figure 5. Example of simulated influence of surface fluxes in Europe at NOR and SMR

We represent in Figure 6 the average of the hourly surface flux and background errors by station; to compute the average, we actually take the mean of the variances for a given station, and then take the square root. A few outliers appear in terms of background errors and emission errors. LMP and FKL are stations very close to the South of the domain; such locations will be strongly influenced by any discrepancy in the CAMS-derived background, hence their high overall background errors. Background errors arise from lateral boundary conditions being slightly different between models as they do not have the exactly same horizontal extent and from different transport of background concentrations within the domain. HEI, IPR and JUE stations have very strong surface flux errors, proving that the transport models have difficulties to represent properly emission (or sink) influence to these stations. HEI station is nearby the city of Heidelberg, with strong anthropogenic emissions in pixels nearby the station, proving difficult to represent in a consistent manner. Similarly, IPR is a site close to the Milano metropolis, with strong anthropogenic sources. Moreover, IPR is on a mountain ridge on the foothills of the Alps mountains, making it particularly challenging to represent in transport models. JUE is a countryside site, in Western Germany, nearby the Belgium and Netherlands borders. This site is influenced by both strong anthropogenic and biogenic fluxes which prove challenging to represent in a consistent manner by models; this

is explained by strong surface fluxes in the same grid cells as the station, inducing large aggregation errors in the models. This would be related to the fact that models experience more difficulty to represent source-receptor relationship close to emission hotspots, rather than long-range transport across Europe.

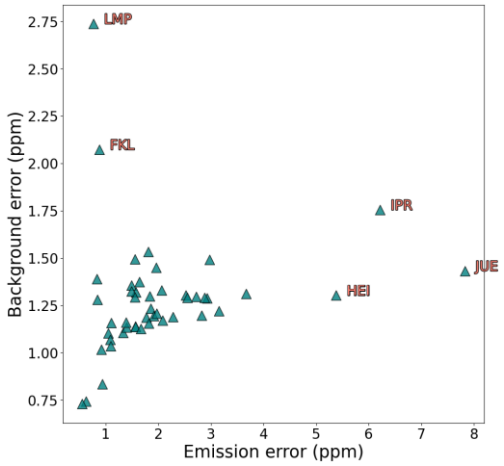

Figure 6. Average emission and background uncertainty defined by model spread for each station. All models are used to compute the spread of the emission errors, whereas background errors are computing based on four models only as STILT do not compute the influence of the background. Outliers are identified by their ID.

6.2 Inversion outputs

As mentioned in Sect. 4, we carried out 6 inversion experiments with different combinations of models and inversion methods, with all the rest of the configuration being identical. We present below how the different combinations perform compared to each other and how much their results deviate.

6.2.1 Posterior fit to observations

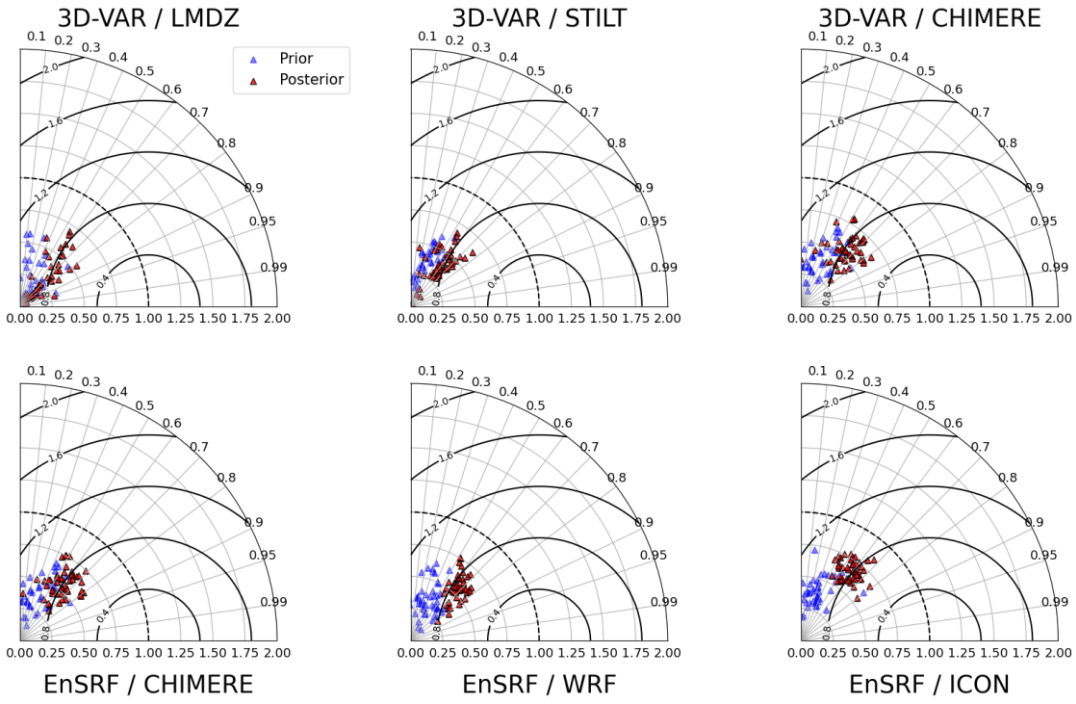

Figure 7. Taylor plot for each inversion method and model and for prior and posterior simulations.

We present de-seasonalized Taylor plots for each combination of inversion method and transport model. Each point represents one station. All model under-estimate the variability of the observations in general. In particular, LMDZ has the smallest variability of all models, which is explained by the much lower resolution of the global model, compared to regional models.

In all cases, posterior simulations are improved compared to prior, with no model clearly better than the other.

6.2.2 Comparison of posterior fluxes

Figure 8 compares posterior flux increments for each combination of inversion method and transport model, aggregated at the quarterly scale. 3D-VAR methods compute smooth increments relative to the 200 km correlation length prescribed in the inversions. By comparison, EnSRF results are very noisy, relative to the relatively small number of members compared to our application case at 0.1°x0.1° resolution. Nevertheless, posterior increments are overall consistent, with overall positive increments in summer over Europe. To reduce the noise in EnSRF results, one approach is to apply localization. While localization is available in the CIF, we have not utilized it here due to the need for further testing.

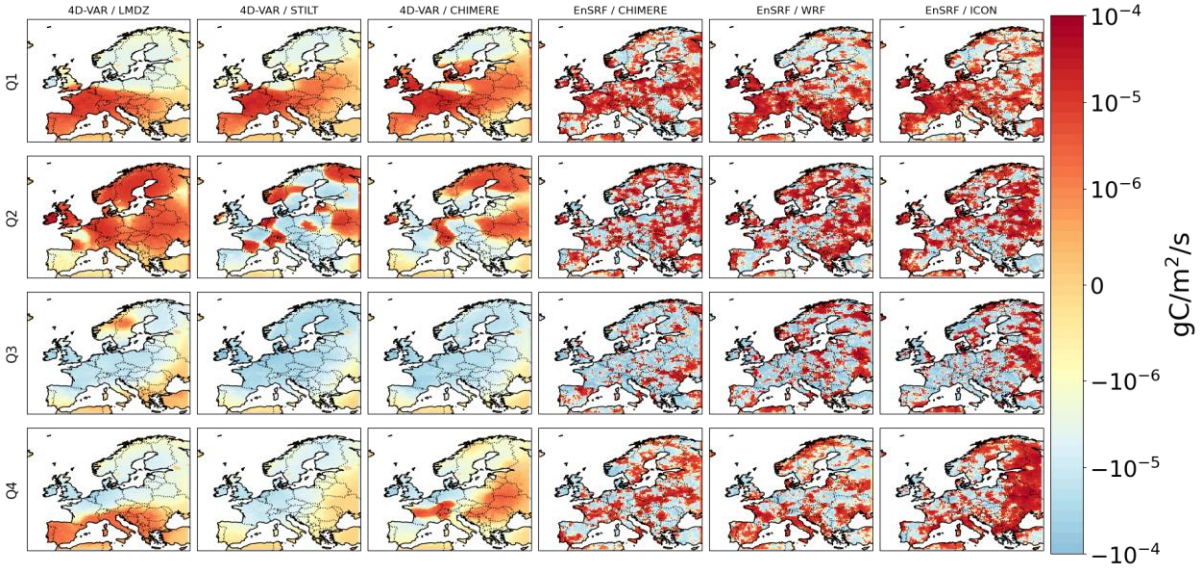

Figure 8. Comparison of posterior increments per quarter of the year 2019 and by inversion method and model.

In Figure 9, we represent time series of posterior fluxes compared to prior fluxes. All model/method combinations point to a shifted seasonal cycle compared to the prior. The maximum vegetation uptake is simulated in June or July after inversion, rather than in April or May prior to the inversion. In most regions, the inversion results are outside the prior uncertainties, pointing to a strong influence of observations, compared to the prior. When using the χ^2 statistics, we find a range of 2.5-10 for the various cases. As a reminder, the χ^2 statistics should ideally have a value of 1 if all statistics (in particular the observation and control vectors uncertainty matrices) are well defined. To fulfil the χ^2 requirement, one would need to multiply both observation and control vector uncertainties by $\sqrt{\chi^2}$. In such a case, the prior uncertainties would be increased by 50% to 300%, as well as observations. Thus, the inversions would limit the impact of observations and posterior fluxes would remain within the range of prior uncertainties.

Further experiments should be carried out to confirm that aspect, but the dense network in Europe allows the inversion to deduce posterior fluxes with little influence from the prior. This is not true for all regions, such as the Iberian peninsula, where no station is available and for which inversions do not deviate significantly and consistently from the background.

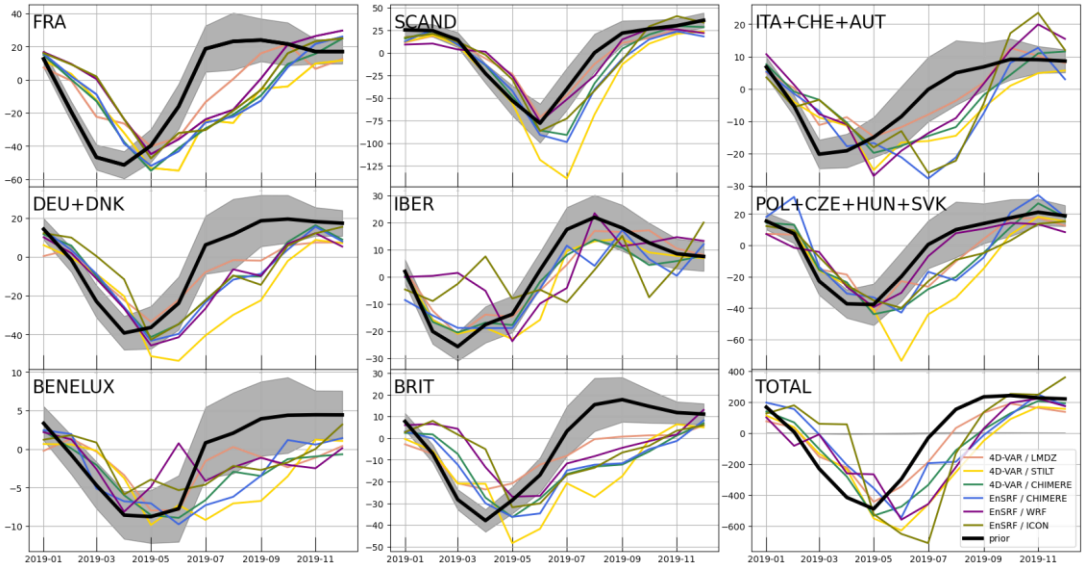

Figure 9. Time series of prior and posterior natural fluxes by country and groups of countries. FRA=France, DEU=Germany, BENELUX=Belgium+The Netherlands+Luxembourg, SCAND=Norway+Sweden+Finland, IBER=Spain+Portugal, BRIT=United Kingdom+Ireland, ITA=Italie, CHE=Switzerland, AUT=Austria, POL=Poland, CZE=Czech Republic, HUN=Hungary, SVK=Slovakia.

In regions with a dense network, the spread between inversions is generally smaller than the prior uncertainties. This points to a limited influence of the transport model and inversion method on the inversion results. This does not hold for regions with sparse networks such as the Iberian and Italian peninsulas.

7 Conclusion

In conclusion, this report presents the outcomes of a rigorous inter-comparison of models and inversion approaches facilitated by the Community Inversion Framework (CIF). Our focus was on an inversion study over Europe aimed at quantifying CO2 surface fluxes for the year 2019, utilizing surface measurements. Employing LMDZ, CHIMERE, STILT, ICON-ART, and WRF-Chem, along with variational and Ensemble Square-Root filter inversion methods, our analysis revealed pronounced challenges associated with transport and methodology errors at the pixel scale, thereby limiting detailed analysis of CO2 inversion fluxes at the European scale to larger regions.

Nevertheless, at the country scale, our findings indicate a general concordance among inversions employing different transport models and methods, particularly in regions proximate to the denser sections of the ICOS network. Notably, all inversions align on a peak vegetation uptake in June, contrasting with the prior model's assertion of May.

The traceability and comparability assured by CIF for inversion cases greatly facilitate community-wide inter-comparison exercises, given the identical nature of all operations within the system, except for the transport model itself or the inversion method. This establishes a foundation for systematic and consistent assessment of uncertainties in inversions, laying the groundwork for future reporting.

Furthermore, we advocate for the widespread adoption of CIF as a fundamental component in upcoming emission monitoring systems. CIF's distinguishing feature lies in its efficient computation of the impact of both transport and methodological errors, an attribute particularly vital at smaller scales where uncertainties are more pronounced.

To fortify inversion practices, we propose the inversion community embraces standardized methodologies and guidelines. A pivotal recommendation involves integrating systematic benchmark tests tailored to each application study. Our study emphasizes the significance of incorporating multiple transport models and inversion methods in these benchmarking processes, a multifaceted approach crucial for a comprehensive evaluation of the reliability of inversion results in specific application cases.

8 References

- Baker, D. F., Law, R. M., Gurney, K. R., Rayner, P., Peylin, P., Denning, A. S., Bousquet, P., Bruhwiler, L., Chen, Y.-H., Ciais, P., Fung,I. Y., Heimann, M., John, J., Maki, T., Maksyutov, S., Masarie, K., Prather, M., Pak, B., Taguchi, S., and Zhu, Z.: TransCom 3 inversion intercomparison: Impact of transport model errors on the interannual variability of regional CO2 fluxes, 1988–2003, Global Biogeochem. Cycles, 20, GB1002, https://doi.org/10.1029/2004GB002439, 2006.
- Basu, S., Baker, D. F., Chevallier, F., Patra, P. K., Liu, J., and Miller, J. B.: The impact of transport model differences on CO2 surface flux estimates from OCO-2 retrievals of column average CO2, Atmos. Chem. Phys., 18, 7189–7215, https://doi.org/10.5194/acp-18-7189-2018, 2018.
- Beck, V., Koch, T., Kretschmer, R., Ahmadov, R., Gerbig, C., Marshall, J., Pillai, D., and Heimann, M.: The WRF Greenhouse Gas Model (WRF-GHG), Technical Report No. 25, techreport 25, Max Planck Institute for Biogeochemistry, https://www.bgc-jena.mpg.de/bgc-systems/pmwiki2/uploads/Download/Wrf-ghg/WRF-GHG_Techn_Report.pdf, 2011.
- Berchet, A., Sollum, E., Thompson, R. L., Pison, I., Thanwerdas, J., Broquet, G., Chevallier, F., Aalto, T., Berchet, A., Bergamaschi, P., Brunner, D., Engelen, R., Fortems-Cheiney, A., Gerbig, C., Groot Zwaaftink, C. D., Haussaire, J.-M., Henne, S., Houweling, S., Karstens, U., Kutsch, W. L., Luijkx, I. T., Monteil, G., Palmer, P. I., van Peet, J. C. A., Peters, W., Peylin, P., Potier, E., Rödenbeck, C., Saunois, M., Scholze, M., Tsuruta, A., and Zhao, Y.: The Community Inversion Framework v1.0: a unified system for atmospheric inversion studies, Geosci. Model Dev., 14, 5331–5354, https://doi.org/10.5194/gmd-14-5331-2021, 2021.
- Berchet Antoine, Espen Sollum, Isabelle Pison, Rona L. Thompson, Joël Thanwerdas, Audrey Fortems-Cheiney, Jacob C. A. van Peet, Elise Potier, Frédéric Chevallier, Grégoire Broquet, & Adrien Berchet. (2022). The Community Inversion Framework: codes and documentation (v1.1). Zenodo. https://doi.org/10.5281/zenodo.6304912
- Broquet, G., Chevallier, F., Bréon, F.-M., Kadygrov, N., Alemanno, M., Apadula, F., Hammer, S., Haszpra, L., Meinhardt, F., Morguí, J. A., Necki, J., Piacentino, S., Ramonet, M., Schmidt, M., Thompson, R. L., Vermeulen, A. T., Yver, C., and Ciais, P.: Regional inversion of CO2 ecosystem fluxes from atmospheric measurements: reliability of the uncertainty estimates, Atmos. Chem. Phys., 13, 9039–9056, https://doi.org/10.5194/acp-13-9039-2013, 2013.
- Chevallier, F., et al. (2010), CO2 surface fluxes at grid point scale estimated from a global 21 year reanalysis of atmospheric measurements, J. Geophys. Res., 115, D21307, doi:10.1029/2010JD013887.
- Chevallier, F., Remaud, M., O'Dell, C. W., Baker, D., Peylin, P., and Cozic, A.: Objective evaluation of surface- and satellite-driven carbon dioxide atmospheric

inversions, Atmospheric Chemistry and Physics, 19, 14 233–14 251, https://doi.org/https://doi.org/10.5194/acp-19-14233-2019, 2019.

- Crowell, S., et al., The 2015–2016 carbon cycle as seen from OCO-2 and the global in situ network, Atmos. Chem. Phys., 19, 9797–9831, https://doi.org/10.5194/acp-19-9797-2019 (2019)
- Engelen, R. J., Denning, A. S., and Gurney, K. R.: On error estimation in atmospheric CO2 inversions, Journal of Geophysical Re-search: Atmospheres, 107, ACL 10–1–ACL 10–13, https://doi.org/10.1029/2002JD002195, 2002.
- Fortems-Cheiney, A., Pison, I., Broquet, G., Dufour, G., Berchet, A., Potier, E., Coman, A., Siour, G., and Costantino, L.: Variational regional inverse modeling of reactive species emissions with PYVAR-CHIMERE-v2019, Geosci. Model Dev., 14, 2939–2957, https://doi.org/10.5194/gmd-14-2939-2021, 2021.
- Gilbert, J.C., Lemaréchal, C. Some numerical experiments with variable-storage quasi-Newton algorithms. Mathematical Programming 45, 407–435 (1989). https://doi.org/10.1007/BF
- Grell GA, SE Peckham, R Schmitz, and SA McKeen, G Frost, WC Skamarock, and B Eder. 2005. Fully coupled 'online' chemistry in the WRF model. Atmos. Environ., 39:6957-6976.
- Gurney, K. R., Law, R. M., Denning, A. S., Rayner, P. J., Baker, D., Bousquet, P., Bruhwiler, L., Chen, Y.-H., Ciais, P., Fan, S., Fung, I. Y., Gloor, M., Heimann, M., Higuchi, K., John, J., Maki, T., Maksyutov, S., Masarie, K., Peylin, P., Prather, M., Pak, B. C., Randerson, J.,Sarmiento, J., Taguchi, S., Takahashi, T., and Yuen, C. W.: Towards robust regional estimates of CO2 sources and sinks using atmospheric transport models, Nature, 415, 626–630, https://doi.org/10.1038/415626a, 2002.
- Gurney, K. R., Law, R. M., Denning, A. S., Rayner, P. J., Baker, D., Bousquet, P., Bruhwiler, L., Chen, Y.-H., Ciais, P., Fan, S., Fung, I. Y.,Gloor, M., Heimann, M., Higuchi, K., John, J., Kowalczyk, E., Maki, T., Maksyutov, S., Peylin, P., Prather, M., Pak, B. C., Sarmiento, J., Taguchi, S., Takahashi, T., and Yuen, C.-W.: TransCom 3 CO2 inversion intercomparison: 1. Annual mean control results and sensitivity5to transport and prior flux information, Tellus B, 55, 555–579, https://doi.org/10.1034/j.1600-0889.2003.00049.x, 2003.
- Hersbach, H., Bell, B., Berrisford, P., Biavati, G., Horányi, A., Muñoz Sabater, J., Nicolas, J., Peubey, C., Radu, R., Rozum, I., Schepers, D., Simmons, A., Soci, C., Dee, D., Thépaut, J-N. (2023): ERA5 hourly data on single levels from 1940 to present. Copernicus Climate Change Service (C3S) Climate Data Store (CDS), DOI: 10.24381/cds.adbb2d47
- ICOS RI, Bergamaschi, P., Colomb, A., De Mazière, M., Emmenegger, L., Kubistin, D., Lehner, I., Lehtinen, K., Lund Myhre, C., Marek, M., Platt, S.M., Plaß-Dülmer, C., Schmidt, M., Apadula, F., Arnold, S., Blanc, P.-E., Brunner, D., Chen, H., Chmura, L., Conil, S., Couret, C., Cristofanelli, P., Delmotte, M., Forster, G., Frumau, A., Gheusi, F., Hammer, S., Haszpra, L., Heliasz, M., Henne, S., Hoheisel, A., Kneuer, T., Laurila, T., Leskinen, A., Leuenberger, M., Levin, I., Lindauer, M., Lopez, M., Lunder, C., Mammarella, I., Manca, G., Manning, A., Marklund, P., Martin, D., Meinhardt, F., Müller-Williams, J., Necki, J., O'Doherty, S., Ottosson-Löfvenius, M., Philippon, C., Piacentino, S., Pitt, J., Ramonet, M., Rivas-Soriano, P., Scheeren, B., Schumacher, M., Sha, M.K., Spain, G., Steinbacher, M., Sørensen, L.L., Vermeulen, A., Vítková, G., Xueref-Remy, I., di Sarra, A., Conen, F., Kazan, V., Roulet, Y.-A., Biermann, T., Heltai, D., Hensen, A., Hermansen, O., Komínková, K., Laurent, O., Levula, J., Pichon, J.-M., Smith, P., Stanley, K., Trisolino, P., ICOS Carbon Portal, ICOS Atmosphere Thematic Centre, ICOS Flask And Calibration Laboratory, ICOS Central Radiocarbon Laboratory, 2023. European Obspack compilation of atmospheric carbon dioxide data from ICOS and non-ICOS European stations for the period 1972-2022; obspack_co2_466_GLOBALVIEWplus_v8.0_2023-03-08. https://doi.org/10.18160/CEC4-CAGK

- Jähn, M., Kuhlmann, G., Mu, Q., Haussaire, J.-M., Ochsner, D., Osterried, K., Clément, V., and Brunner, D.: An online emission module for atmospheric chemistry transport models: implementation in COSMO-GHG v5.6a and COSMO-ART v5.1-3.1, Geoscientific Model Development, 13, 2379–2392, https://doi.org/10.5194/gmd-13-2379-2020, 2020.
- Law, R. M., Chen, Y.-H., Gurney, K. R., and 3 Modellers, T.: TransCom 3 CO2 inversion intercomparison: 2. Sensitivity of annual mean results to data choices, Tellus B, 55, 580–595, https://doi.org/10.1034/j.1600-0889.2003.00053.x, 2003.
- McGrath, M. J., Petrescu, A. M. R., Peylin, P., Andrew, R. M., Matthews, B., Dentener, F., Balkovič, J., Bastrikov, V., Becker, M., Broquet, G., Ciais, P., Fortems-Cheiney, A., Ganzenmüller, R., Grassi, G., Harris, I., Jones, M., Knauer, J., Kuhnert, M., Monteil, G., Munassar, S., Palmer, P. I., Peters, G. P., Qiu, C., Schelhaas, M.-J., Tarasova, O., Vizzarri, M., Winkler, K., Balsamo, G., Berchet, A., Briggs, P., Brockmann, P., Chevallier, F., Conchedda, G., Crippa, M., Dellaert, S. N. C., Denier van der Gon, H. A. C., Filipek, S., Friedlingstein, P., Fuchs, R., Gauss, M., Gerbig, C., Guizzardi, D., Günther, D., Houghton, R. A., Janssens-Maenhout, G., Lauerwald, R., Lerink, B., Luijkx, I. T., Moulas, G., Muntean, M., Nabuurs, G.-J., Paquirissamy, A., Perugini, L., Peters, W., Pilli, R., Pongratz, J., Regnier, P., Scholze, M., Serengil, Y., Smith, P., Solazzo, E., Thompson, R. L., Tubiello, F. N., Vesala, T., and Walther, S.: The consolidated European synthesis of CO2 emissions and removals for the European Union and United Kingdom: 1990–2020, Earth Syst. Sci. Data, 15, 4295–4370, https://doi.org/10.5194/essd-15-4295-2023, 2023.
- Monteil, G., Broquet, G., Scholze, M., Lang, M., Karstens, U., Gerbig, C., Koch, F.-T., Smith, N. E., Thompson, R. L., Luijkx, I. T., White, E., Meesters, A., Ciais, P., Ganesan, A. L., Manning, A., Mischurow, M., Peters, W., Peylin, P., Tarniewicz, J., Rigby, M., Rödenbeck, C., Vermeulen, A., and Walton, E. M.: The regional European atmospheric transport inversion comparison, EUROCOM: first results on European-wide terrestrial carbon fluxes for the period 2006–2015, Atmos. Chem. Phys., 20, 12063–12091, https://doi.org/10.5194/acp-20-12063-2020, 2020.
- Patra, P. K., Houweling, S., Krol, M., Bousquet, P., Belikov, D., Bergmann, D., Bian, H., Cameron-Smith, P., Chipperfield, M. P., Corbin,K., Fortems-Cheiney, A., Fraser, A., Gloor, E., Hess, P., Ito, A., Kawa, S. R., Law, R. M., Loh, Z., Maksyutov, S., Meng, L., Palmer,P. I., Prinn, R. G., Rigby, M., Saito, R., and Wilson, C.: TransCom model simulations of CH4 and related species: linking transport,surface flux and chemical loss with CH4 variability in the troposphere and lower stratosphere, Atmos. Chem. Phys., 11, 12 813–12 837, https://doi.org/10.5194/acp-11-12813-2011, 2011.
- Peylin, P., Law, R. M., Gurney, K. R., Chevallier, F., Jacobson, A. R., Maki, T., Niwa, Y., Patra, P. K., Peters, W., Rayner, P. J., Rödenbeck, C.,van der Laan-Luijkx, I. T., and Zhang, X.: Global atmospheric carbon budget: results from an ensemble of atmospheric CO2 inversions, Biogeosciences, 10, 6699–6720, https://doi.org/10.5194/bg-10-6699-2013, 2013.
- Remaud, M., Chevallier, F., Cozic, A., Lin, X., and Bousquet, P., On the impact of recent developments of the LMDz atmospheric general circulation model on the simulation of CO2 transport, Geosci. Model Dev., 11, 4489–4513,https://doi.org/10.5194/gmd-11-4489-2018 (2018).
- Rödenbeck, C., Bakker, D. C. E., Metzl, N., Olsen, A., Sabine, C., Cassar, N., Reum, F., Keeling, R. F., and Heimann, M.: Interannual sea–air CO2 flux variability from an observation-driven ocean mixed-layer scheme, Biogeosciences, 11, 4599–4613, https://doi.org/10.5194/bg-11-4599-2014, 2014.
- Skamarock, W. C., J. B. Klemp, J. Dudhia, D. O. Gill, Z. Liu, J. Berner, W. Wang, J. G. Powers, M. G. Duda, D. M. Barker, and X.-Y. Huang, 2019: A Description of the Advanced Research WRF Version 4. NCAR Tech. Note NCAR/TN-556+STR, 145 pp. doi:10.5065/1dfh-6p97

- Steinbach, J., Gerbig, C., Rödenbeck, C., Karstens, U., Minejima, C., and Mukai, H.: The CO2 release and Oxygen uptake from Fossil Fuel Emission Estimate (COFFEE) dataset: effects from varying oxidative ratios, Atmos. Chem. Phys., 11, 6855–6870, https://doi.org/10.5194/acp-11-6855-2011, 2011.
- van der Laan-Luijkx, I. T., van der Velde, I. R., van der Veen, E., Tsuruta, A., Stanislawska, K., Babenhauserheide, A., Zhang, H. F., Liu, Y., He, W., Chen, H., Masarie, K. A., Krol, M. C., and Peters, W.: The CarbonTracker Data Assimilation Shell (CTDAS) v1.0: implementation and global carbon balance 2001–2015, Geosci. Model Dev., 10, 2785–2800, https://doi.org/10.5194/gmd-10-2785-2017, 2017.
- Yadav, V. and Michalak, A. M.: Improving computational efficiency in large linear inverse problems: an example from carbon dioxide flux es-timation, Geoscientific Model Development, 6, 583–590, https://doi.org/https://doi.org/10.5194/gmd-6-583-2013, 2013
- Zängl, G., Reinert, D., Rípodas, P., and Baldauf, M.: The ICON (ICOsahedral Non-hydrostatic) modelling framework of DWD and MPI-M: description of the non-hydrostatic dynamical core, Q. J. Roy. Meteor. Soc., doi:10.1002/qj.2378, online first, 2014. 569

Document History

Version	Author(s)	Date	Changes
	Name (Organisation)	dd/mm/yyyy	

Internal Review History

Internal Reviewers	Date	Comments
Name (Organisation)	dd/mm/yyyy	
Wouter Peters (WUR)	14/11/2023	Yes and addressed